

1 Article type: Research paper
2 Date text revised/resubmitted: June 2019
3 Number of words in your main text and tables: ~ 7,800
4 Number of figures: 11
5 Number of tables: 2

6 -----

7 **Influence of Geology and Hydrogeology on Heat Rejection from Residential Basements in**
8 **Urban Areas**

9 Author 1

10 Asal Bidarmaghz✉, PhD

11 Lecturer in Geotechnical Engineering

12 School of Civil and Environmental Engineering, University of New South Wales, Sydney, Australia

13

14 Author 2

15 Ruchi Choudhary, PhD

16 Reader in Architectural Engineering

17 Department of Engineering, University of Cambridge, Trumpington Street CB2 1PZ, UK

18

19 Author 3

20 Kenichi Soga, PhD

21 Chancellor's Professor

22 Department of Civil and Environmental Engineering, University of California, Berkeley, USA

23

24 Author 4

25 Holger Kessler, MSc, FGS

26 British Geological Survey, Keyworth, Nottingham NG12 5GG, UK

27

28 Author 5

29 Ricky L. Terrington, MSc, CGeog (GIS)

30 British Geological Survey, Keyworth, Nottingham NG12 5GG, UK

31

32 Author 6

33 Stephen Thorpe, BSc

34 British Geological Survey, Keyworth, Nottingham NG12 5GG, UK

35

36 **Full contact details of the corresponding author**

37 Asal Bidarmaghz, Lecturer in Geotechnical Engineering

38 School of Civil and Environmental Engineering, University of New South Wales, Sydney, Australia

39 E-mail: a.bidarmaghz@unsw.edu.au

40 **Abstract**

41 Urbanization and limited land availability have resulted in the increased utilization of underground structures
42 including residential basements in largely populated cities such as London, with an average addition of 200
43 basements per year in some boroughs. Residential basements kept at a comfortable temperature level throughout
44 the year significantly contribute to heat fluxes in the subsurface as well as an increase in ground temperature.
45 Understanding the ground thermal status is crucial in managing the significant geothermal energy potential in
46 urban areas as well as the sustainable development of the urban underground, and in maintaining the energy
47 efficiency of underground structures. In this proof-of-concept study, a 3D finite element approach accounting for
48 coupled heat transfer and fluid flow in the ground was used to investigate the influence of ground conditions on
49 the heat rejection rate from basements. A detailed analysis was made of ground, above ground and underground
50 built environment characteristics. This study demonstrates that the amount of heat from basements rejected to the
51 ground constitutes a significant percentage of the total heat loss from buildings, particularly in the presence of
52 groundwater flow. The extent of thermal disturbance in the ground varies depending on the ground characteristics.
53 The volume of ground thermal disturbance inversely correlates with the groundwater flow rate in the ground
54 mainly consisting of granular (highly permeable) material. However, a direct correlation exists when the thickness
55 of the granular layer decreases. A larger horizontal to vertical ratio of ground thermal disturbance is observed
56 when the thickness of the permeable layer increases.

57 **List of Notations**

A_s	annual air swing [$^{\circ}\text{C}$]
$C_{p,f}$	groundwater specific heat capacity [J/kgK]
$C_{p,m}$	solid material specific heat capacity [J/kgK]
\mathbf{g}	gravitational acceleration vector [m/s^2]
K	ground permeability [m^2]
k_h	ground hydraulic conductivity [m/s]
k_v	vegetation coefficient [-]
n	porosity [-]
p_f	pore pressure [Pa]
t	time of the year [day]
t_0	coldest temperature day from January 1 st [day]
$T_{\text{ground, mean}}$	ground annual average temperature [$^{\circ}\text{C}$]
T_m	temperature field in the ground [$^{\circ}\text{C}$]
\mathbf{v}_f	groundwater velocity [m/s]
z	depth in the ground [m]
α	ground thermal diffusivity [m^2/s]
λ_{eff}	effective thermal conductivity of porous ground [W/mK]
λ_f	groundwater thermal conductivity [W/mK]
λ_m	solid material thermal conductivity [W/mK]
μ_f	groundwater dynamic viscosity [$\text{Pa}\cdot\text{s}$]
ρ_f	groundwater density [kg/m^3]
ρ_m	solid material density [kg/m^3]

58 **Keywords**

59 geothermal energy, basements, groundwater, geology, finite element modelling, urban subsurface.

60 1. Introduction

61 Current rates of urbanization predict that 70% of the world's population will live in cities by 2050 (Un-Habitat,
62 2012). In addition to the above-ground landscape, underground built environments are an important feature of
63 urbanization. In densely populated cities, where land is precious and planning laws constrain residential
64 extensions above ground, underground spaces are attractive for different purposes, most commonly for transport
65 and residential purposes. A review of recent planning applications for residential basements in London shows that
66 basements which were used as cellars, storerooms and/or kitchens, are now mainly retrofitted to self-confined
67 living flats or as an extension to the rest of the house providing additional living/leisure spaces¹²³⁴. These
68 residential basements are likely to be kept at a comfortable temperature (18°C)⁵ throughout the year. Given
69 London's climate, where the annual average ground temperature is relatively low (12°C-14°C, (Price et al., 2018))
70 it is likely that residential basements continuously reject heat to the ground. A large increase in the number of
71 heated basements in an urban area can thus result in a rise in temperature in the surrounding ground in the long
72 term, especially in the presence of groundwater flow as it dissipates the heat away from the basements in the
73 direction of groundwater flow affecting a greater volume in the ground. The heat flux from a large number of
74 basements into the ground accelerates the creation of an Urban Underground Heat Island (UUHI), where the
75 ground is significantly warmer than its surroundings. The elevated ground temperature can be economically and
76 environmentally advantageous in terms of geothermal energy exploitation. It is shown that the geothermal
77 potential of urban areas is on average about 50% higher than in rural areas and can exceed the annual residential
78 thermal demand in many urban areas (Zhang et al., 2014). Therefore, understanding the ground thermal
79 disturbance in the urban underground is crucial to facilitate and manage geothermal energy exploitation in a
80 sustainable manner (Arola and Korkka-Niemi, 2014, Zhu et al., 2010, Benz et al., 2015a, Menberg et al., 2013,
81 Zhang et al., 2014, Herbert et al., 2013, Barla et al., 2018).

82 UUHI and its impact on underground climate, in particular, groundwater flow network and temperature have been
83 studied in various cities (Attard et al., 2016a, Epting and Huggenberger, 2013, Menberg et al., 2013, Benz et al.,
84 2015b, Attard et al., 2016b, Taniguchi et al., 2009, Ferguson and Woodbury, 2007, Ferguson and Woodbury,
85 2004, Epting et al., 2017, Epting et al., 2013). The heat flux into the subsurface as the heat input into shallow
86 urban aquifers is caused by various anthropogenic heat sources. This includes increased ground surface
87 temperature, solar radiation, buildings and basements, road tunnels, sewage networks, subway systems,
88 reinjections of thermal wastewater and other geothermal energy systems such as ground source heat pumps
89 (GSHPs). Buildings and basements are reported to have a significant impact on subsurface temperature with the
90 maximum heat flux of between 10 W/m² and 16 W/m² (Menberg et al., 2013, Epting and Huggenberger, 2013,
91 Mueller et al., 2018).

92 Despite detailed studies on underground structures and heat rejection to the subsurface in various cities (Rivera et
93 al., 2017, Ferguson and Woodbury, 2004, Ferguson and Woodbury, 2007), the focus of most past research has
94 been on identifying anthropogenic heat sources and quantifying the heat flux to the subsurface, as well as the
95 consequent subsurface temperature increase via analytical and numerical approaches. Underground structures are
96 significant contributors to subsurface temperature increase, and heat loss from these structures to the ground
97 largely varies in different studies. However, to what extent ground conditions influence heat flux from
98 underground structures to the subsurface has been mostly overlooked. This is due to the lack of detailed knowledge
99 of the subsurface (e.g., limited ground temperature measurements, spatial heterogeneity of thermal conditions of
100 the ground, the scale and complexity of the problem, etc.) (Vázquez Suñé et al., 2016). The lack of reliable
101 knowledge about urban underground has led to energy inefficiency in a number of structures. The high

¹ Arup 2008. Royal Borough of Kensington and Chelsea Town Planning Policy on Subterranean Development: Phase1-Scoping Study. London, UK.

² Baxter, A. 2013. Royal Borough of Kensington and Chelsea Residential Basement Study Report. London, UK.

³ RBKC 2014. Basements Development Data: Partial Review of the Core Strategy. London, UK.

⁴ RBKC 2009. Subterranean Development: Supplementary Planning Document. London, UK.

⁵ Lane, M. 2011. How warm is your home. BBC Magazine. UK.

102 temperature in some underground train lines around the world and the passengers' thermal discomfort as a result
103 represents one of the many problems which could have largely been prevented with a better understanding of the
104 ground (Furfano et al., 2018, Ampofo et al., 2004, Cockram and Birnie, 1976, Barla et al., 2016). The aim of this
105 paper is to investigate the extent to which thermally disturbed ground around heated basements is influenced by
106 different geological and hydrogeological conditions. To what extent heat loss from basements and hence their
107 thermal energy demand varies in different ground conditions are also investigated. The heat rejection rate from a
108 set of heated residential basements in three districts with different geological and hydrogeological conditions was
109 numerically modelled. In this study, we selected a representative London borough – The Royal Borough of
110 Kensington and Chelsea (RBKC) – known for its high density of existing residential basements⁶ (Baldwin et al.,
111 2018). The LSOA⁷ sub-divisions of RBKC were examined for their ground geology, the number of residential
112 basements, and hydrogeological properties. From these sub-divisions, three representative areas were selected for
113 analysis and comparison. Each area has a similar number of basements, relatively similar surface area and similar
114 hydraulic head differences. However, each has distinct combinations of geology types (varying between sand,
115 gravel and clay), hence different hydraulic and thermal properties. The dominant building typology and the
116 number of existing basements in RBKC were obtained from a detailed geo-mapping dataset⁸. The basement type
117 and characteristics corresponding to the most dominant building type in the borough were corroborated through
118 a comprehensive and time-consuming review of basement development applications submitted to RBKC planning
119 and building control portal⁹.

120 The geology and hydrogeology of the studied areas were extracted from a complex 3D geological model of RBKC
121 aggregated at relevant resolutions. In this 3D model, the 2D ground hydro-thermal properties were spatially
122 integrated into the model based on the geological classifications. Groundwater flow rate and direction play a key
123 role in the temperature distribution of the ground (Angelotti et al., 2014, Hecht-Méndez et al., 2013). Therefore,
124 representative groundwater level contours were extracted from the groundwater model developed for superficial
125 deposits in RBKC accounting for the lost rivers (i.e., Fleet and Westbourne) as well as the River Thames (British
126 Geological Survey, 2017).

127 **2. Above and underground characteristics of the Royal Borough of Kensington and Chelsea**

128 **2.1.1 Location and typology of basements**

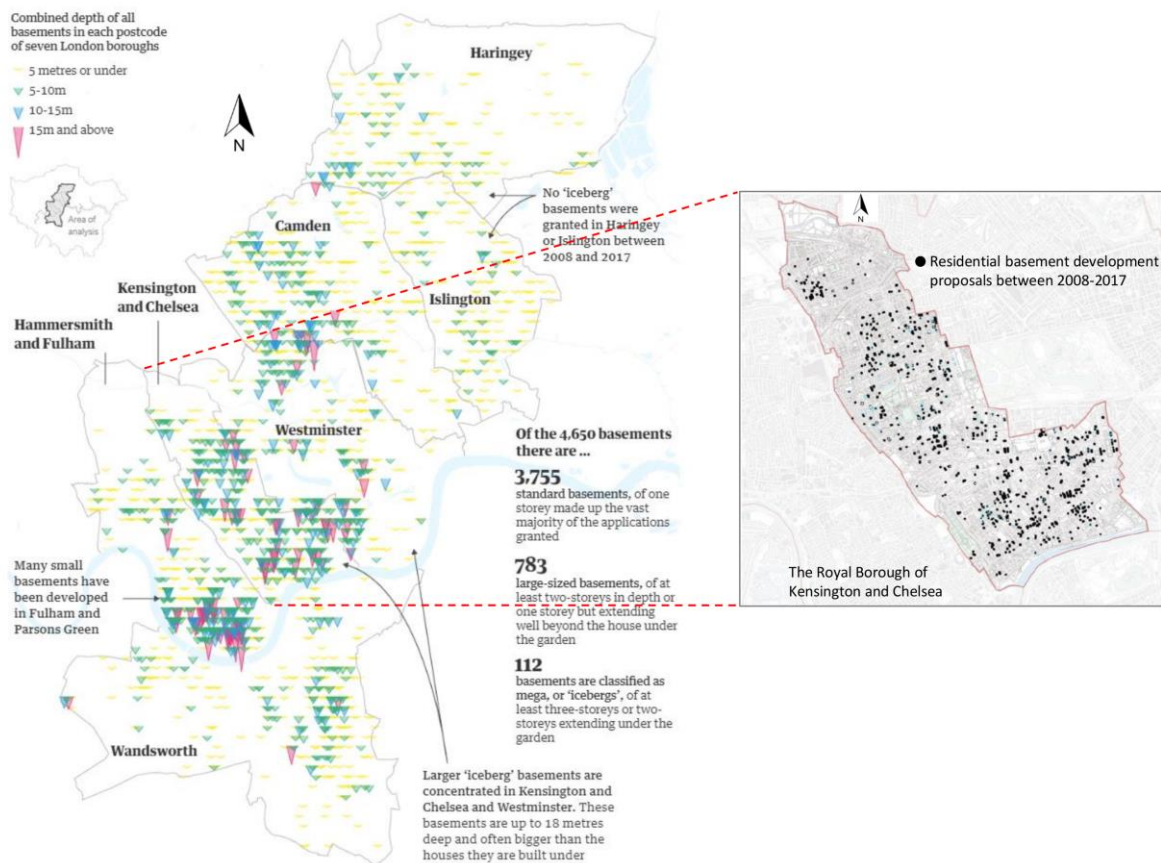
129 The Royal Borough of Kensington and Chelsea (RBKC) is known for large utilization of underground spaces,
130 particularly as residential basements. High land price and construction constraints on above ground extensions
131 have resulted in a significant appetite for underground expansion for residential purposes. Figure 1 shows that
132 about 4,600 basement development proposals were made in seven boroughs in London between 2008-2017
133 (derived from the information provided by each borough's planning portal). About 1,022 approved basement
134 development applications were extracted from RBKC's planning portal between these years (out of 1,300
135 basement development proposals made) demonstrating one of the highest basement development rates per
136 household in the country (see Figure 1). These applications included around 676 standard basements (single
137 storey, mostly under terraced houses), 279 large basements (double storey) and around 67 mega basements (triple
138 storey or more- up to the depth of 18m), where basement developments are spread across the whole borough
139 (Baldwin et al., 2018).

⁶ D. Batty, C. Barr & P. Duncan, (2018). What lies beneath: the subterranean secrets of London's super-rich, The Guardian, UK.

⁷ Lower Layer Super Output Areas (LSOAs) are a geographic hierarchy designed to improve the reporting of small area statistics in England and Wales and are generated to be as consistent in population size as possible. The Minimum population is 1000 and the mean is 1500.

⁸ GeoInformation, (2017a). UK Buildings. Verisk Analytics.

⁹ RBKC, (2018). Planning and Building Control Portal/Planning Search.



140

141

Figure 1. Basement proposals made in seven boroughs in London between 2008-2017 (Baldwin et al., 2018).

142

Reviewing the geo-mapping dataset confirmed the existence of 13,000 known residential basements in RBKC. Building typology, age, material and building height were some of the parameters analysed in this study to gain further insight into the characteristics of residential basements. About 22,000 residential buildings were identified in RBKC, mainly varying between detached and semi-detached houses, flats and terrace houses (see Figure 2).

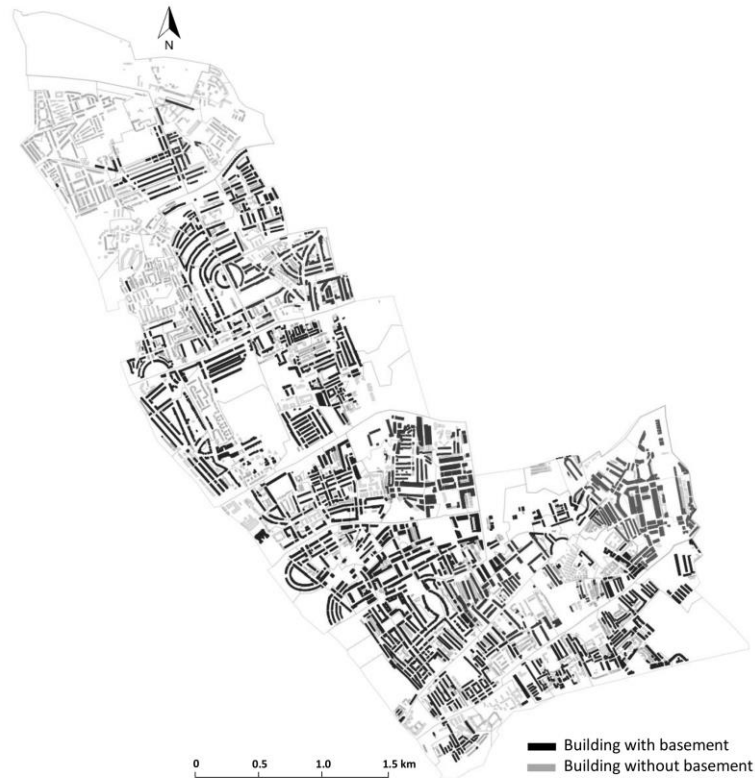
146

Terrace houses are the most dominant building typology in this borough (i.e., 80%) owning 75% (10,000 out of 13,000) of the residential basements in RBKC. Knowing the most dominant building typology (terrace houses) in the borough and their corresponding building age, the characteristics of their basements were investigated by reviewing the basement development applications submitted to the planning and building control portal.

150

A comprehensive review of RBKC's planning and building control portal revealed that for most of the terrace houses, basements are single level and their floor area is similar to the building footprint. Even though RBKC possesses a large number of mega basements (around 200 according to (Baldwin et al., 2018)), these extra-deep basements (~18 m depth) were not the focus of this study as their overall impact on ground temperature on a district scale is negligible (in comparison to 13,000 standard, single-level basements in the borough). In this study, the floor area per standard basement was assumed to be about 50 m², reflecting the basement of a typical two-bedroom terrace house and an average ceiling height of 3 m. A wall and slab thickness of 0.4 m, made of concrete, could be considered standard for these basements. The basements were assumed to be kept at a comfortable temperature level of 18°C throughout the year.

158



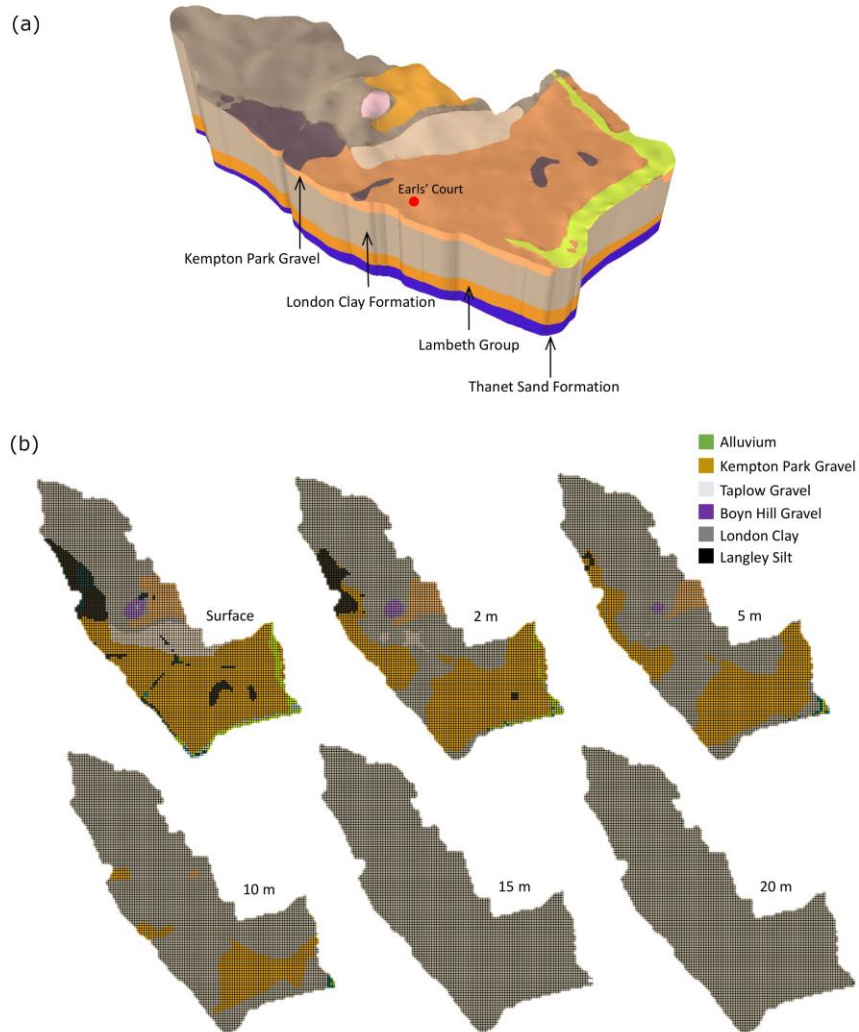
159

160

Figure 2. Residential building distributions in RBKC.

161 A 3D digital geological framework model of London, UK was developed by the British Geological Survey (BGS)
 162 (Burke et al., 2014, Mathers et al., 2014). The geological model was constructed at a scale equivalent to a 1:50 000
 163 scale of 2D geological maps and comprises bedrock, superficial (Quaternary) deposits and artificial ground. It
 164 was constructed using GSI3D modelling software using the modelling procedures described by Kessler et al.
 165 (2009). Existing geological data derived from ground investigation boreholes were digitised using the method
 166 described by Burke et al. (2014).

167 The model developed by BGS for the area of RBKC was based on the 3D geolanduse layer that was a modified
 168 version of the 3D shrink-Swell clays dataset (Jones and Hulbert, 2017), which spans the surface to the top of the
 169 Chalk Group (shown in Figure 3-a). However, the geological layers extending from the surface to the top of the
 170 Lambeth Group was of interest to this work (60-100 m below the ground surface). The 2D hydro-thermal datasets
 171 relevant to the geological classifications of the area were spatially integrated into the 3D model. Each grid cell of
 172 the model contains several characteristics of the ground such as geological units, ground elevation, groundwater
 173 level, hydro-thermal properties, etc. Figure 3-b shows the geological variations within the borough at different
 174 depths from the surface to 20 m depth (reaching the consistent London Clay Formation) using the 50 m x 50 m
 175 grids. Within the first 5 m below the surface, the southern part of the borough mostly consists of permeable River
 176 Terrace Deposits, whereas the northern part sits on impermeable London Clay Formation. However, it is observed
 177 that from about 10 m below the ground surface, the London Clay Formation dominates within the entire borough.



178

179

180

Figure 3. RBKC geology-50 m x 50 m grid (a): 3D geological model, (b): geological variations at different depths (not to scale).

181

182

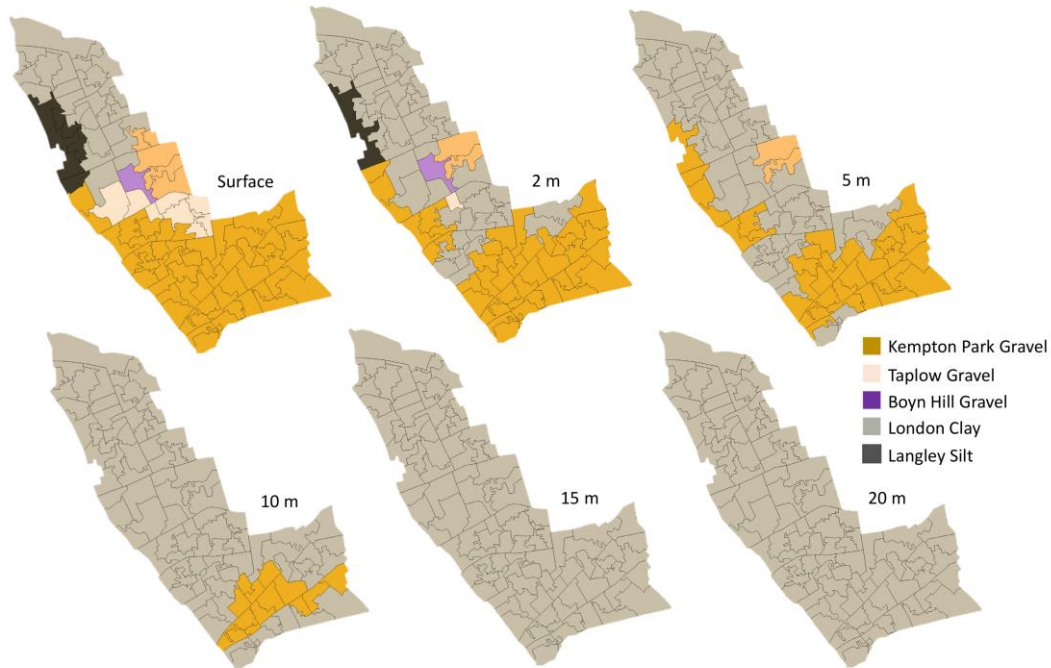
183

184

185

186

The geology of RBKC is relatively consistent (the most significant variation occurs between the south and north part of the borough), therefore, LSOA subdivisions were used as cell grids in this study merging the attributes of 50 m x 50 m grids within each LSOA. By analysing the geological variations of each LSOA at different depths, one dominant geology was selected for each LSOA at a certain depth. Figure 4 shows a summary of the most dominant geological units for different areas of the borough varying by depth at the LSOA level, which shows a similar distribution within the borough as in the 50 m x 50 m grid model (Figure 3).



187

188

Figure 4. RBKC geological classification at LSOA level (not to scale).

189 Different archetypes for the entire Kensington and Chelsea is defined based on the variations in ground geological
 190 conditions. According to Figure 4, four archetypes with various geological classifications by depth have been
 191 identified in the borough as follow:

- 192 • 10 m of River Terrace Deposits underlain by London Clay Formation,
- 193 • 5 m of River Terrace Deposits underlain by London Clay Formation,
- 194 • 2 m of River Terrace Deposits underlain by London Clay Formation,
- 195 • London Clay Formation outcropping at the surface.

196 The River Terrace Deposits are deposits of sands and gravels, which can be up to 10m thick. They are named
 197 differently and have slightly varying characteristics but can all generally be classified as sands and gravels (e.g.,
 198 Kempton Park Gravel).

199 For the purpose of this study and according to the identified geological archetypes, three areas each comprising
 200 LSOAs with similar geology (as shown in Figure 5) were selected as the geological representatives of the borough.
 201 Even though four geological archetypes were initially identified, the area with 2 m of River Terrace Deposits
 202 underlain by London Clay Formation was not studied herein as it was expected to show similar results to the area
 203 where the London Clay Formation outcrops. The three selected areas in RBKC possess similar ground volume
 204 and accommodate almost the same number of residential basements as shown in Figure 5. This was essential to
 205 achieve a consistent $V_{\text{basement}}/V_{\text{ground}}$ (m^3) ratio in all areas and therefore a meaningful comparison within the areas.

206 The three selected areas of RBKC were studied independently by developing a three-dimensional numerical
 207 model of each area with simplified underground heat sources distribution (i.e., basements). The thermal
 208 interaction between neighbouring areas was neglected in order to meet the objective of this paper, which was to
 209 examine the extent of ground temperature disturbance surrounding heated basements as well as the amount of
 210 heat loss variations from the basements to the ground in different ground conditions.



211

212

Figure 5. Three different areas of Kensington and Chelsea selected for modelling.

213 2.1.2 Hydrogeology

214 The groundwater regime across the borough is generally characterised by two distinct aquifers which are separated
 215 by the relatively impermeable London Clay:

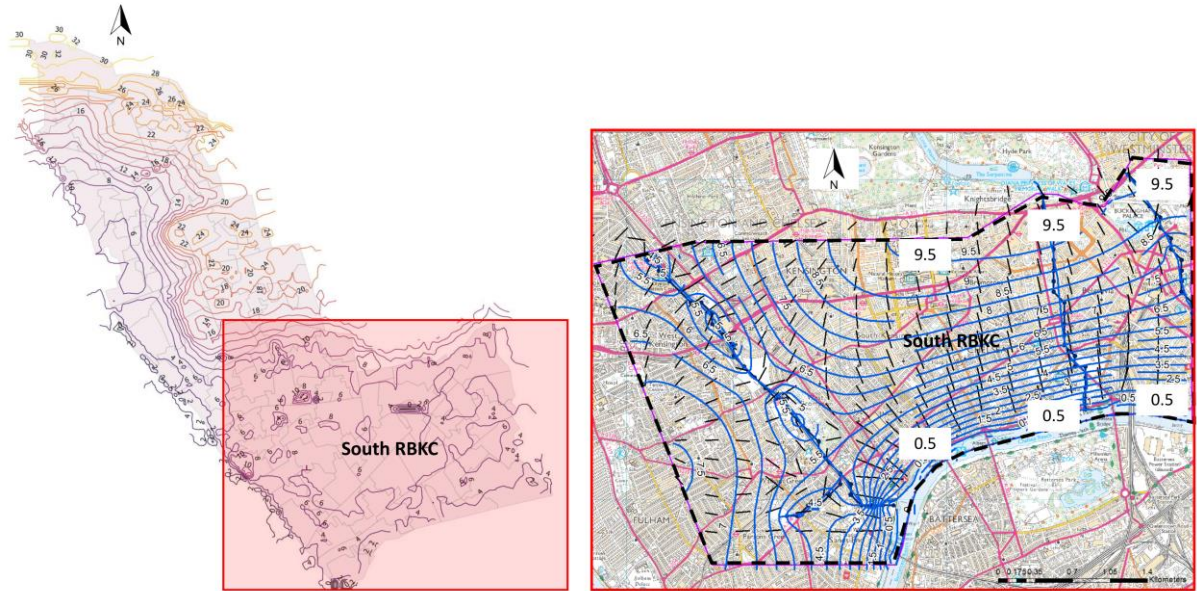
- 216 • the Upper Aquifer is perched water sitting in gravelly soils that overlie the London Clay;
- 217 • the Lower Aquifer within the sandy soils and chalk that lie deep below the London Clay.

218 For basements in the borough, the Upper Aquifer is the relevant aquifer as the extent of ground thermal
 219 disturbance due to its exposure to underground heat sources does not reach the deep aquifer. This is the water
 220 table that would be encountered when digging a basement.

221 The groundwater levels within the shallow aquifer can be extracted from the 3D geological model of RBKC.
 222 Considering the hydraulic conductivity of the superficial deposit and taking into account the lost rivers of Fleet
 223 and Westbourne and the River Thames (with an average recharge rate of 0.12 m/day- derived form BGS' Thames
 224 Basin recharge model), the resulting groundwater level contours are shown in Figure 6 (McKenzie, 2015).

225 According to the groundwater contours, for the southern part of the borough (permeable superficial deposits)
 226 containing studied areas 1 and 2, a slight groundwater flow (around 0.25 m/day with a hydraulic gradient of 0.005)
 227 can be identified. Even though the ground is relatively flat in the southern part of the borough, the water on this
 228 upper aquifer tends to flow slowly on the surface of the London Clay due to the high permeability of River Terrace
 229 Deposits. The northern part of the borough, containing area 3, mainly consists of impermeable London Clay
 230 Formation with negligible groundwater flow in that area.

231 This paper studied the effect of groundwater flow on ground temperature variations and the amount of heat loss
 232 from basements to the ground for different thicknesses of the permeable. Groundwater flow rate is a highly
 233 uncertain parameter, which plays a key role in ground temperature distribution. Therefore, to highlight the
 234 importance of groundwater flow rate on the thermal interaction between basements and the ground, several
 235 groundwater flow rate scenarios varying between 0 m/day (no flow), 0.5 m/day and 1 m/day were considered in
 236 this study by assigning various hydraulic gradient to the models. The extent to which thermally disturbed ground
 237 around a heated basement and the amount of heat loss from basements to the ground are influenced by different
 238 hydrogeological conditions was numerically investigated in detail.



239
 240 Figure 6. Groundwater level contours for the southern part of RBKC (British Geological Survey, 2017).

241 2.1.3 Ground hydro-thermal properties

242 Ground thermal properties are one of the most critical parameters for an accurate estimation of ground thermal
 243 disturbance due to their exposure to heat sources. Ground thermal conductivity and diffusivity used in this study
 244 were obtained from the 3D geological model for RBKC, where the general 2D thermal data classified for different
 245 geological units (mostly gathered from Thermal Response Tasting results around the UK) are spatially integrated
 246 into the model (Price et al., 2018, Busby et al., 2009, British Geological Survey, 2017). The estimated values of
 247 thermal conductivity and diffusivity for Superficial Deposits and London Clay Formation are shown in Table 1.

248 In the presence of groundwater flow, ground hydraulic conductivity plays a significant role in the extent of heat
 249 propagation in the ground exposed to different sources of heat. In this study, the hydraulic conductivity of the
 250 superficial deposit was taken from a case study on the Thames Basin, UK. A conceptual model of superficial
 251 deposits across the Thames Basin was used to define different lithostratigraphic classes of superficial deposits
 252 including River Terrace Deposits. Hydraulic conductivity of the superficial deposits was estimated from grain-
 253 size distribution data, originally collected for mineral resource assessments, using the Kozeny–Carman method
 254 (Burke et al., 2014). The results are shown in Table 1. A relatively low hydraulic conductivity (1×10^{-9} m/s) was
 255 assumed for the impermeable London Clay.

256 Table 1. Estimated thermal/hydraulic conductivity and thermal diffusivity for some of the geological units in RBKC.

Geology		λ [W/(mK)]	α [m ² /s]	k_h [m/s]
Kempton Park Gravel	0-2m depth	0.77	4.5×10^{-7}	4.2×10^{-5}
Kempton Park Gravel	2-10m depth	2.5	9.1×10^{-7}	5.6×10^{-4}
London Clay Formation	Various depths	1.79	9.7×10^{-7}	1×10^{-9}

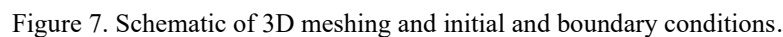
257 3. Thermal modelling of ground exposed to heated basements

258 Using a 3D finite element approach, the three selected areas of RBKC were modelled, accounting for the heated
259 residential basements, ground surface cover, geological variations, and groundwater regime. The finite element
260 package COMSOL Multiphysics was used to couple and solve the equations for conductive and convective heat
261 transfer between the basements and the porous ground. The presented model is a representative of the selected
262 areas in the borough. Each model (three models with the geometry presented in Figure 7) represents one of the
263 three selected areas shown in Figure 5, each with a similar number of basements, similar ground surface area and
264 similar geological and hydrogeological conditions to the real conditions. It should be noted that the exact spatial
265 distributions of basements in each area are simplified into a regular grid consisting of a similar number of
266 basements (800 basements as presented in Figure 7) in the three numerical models. The impact of basements
267 density and distribution on ground temperature elevation is not the focus of this study, hence an even distribution
268 of basements is considered in all three models.

269 3.1.1 Geometry and Meshing

270 Figure 7 shows the finite element representation of the ground exposed to heated basements and the initial and
271 boundary conditions. Each model accommodates about 800 basements in a volume of 1.5 km by 1.5 km by 90 m
272 ground domain. To account for an even distribution of the basements in all models, four batches of 200 basements
273 were considered in this study. The configuration of basement batches was selected randomly. The number of
274 basements assumed in each model was taken from the approximate number of basements currently existing in the
275 three areas shown in Figure 5. These, and their floor areas, were derived from an extensive geospatial database
276 containing footprint information per building and their use, age, and building type¹⁰.

277 A depth of 3 m, including 0.4 m of slab thickness, and wall thickness of 0.4 m were considered for each basement.
278 The floor area per basement was assumed to be 50 m², reflecting a typical two-bedroom terrace house. The entire
279 surface area is meshed by triangular elements consisting of 210,000 elements. To implement efficient swept mesh
280 (prisms) in vertical direction, the model is partitioned in depth into several layers with varying thicknesses, for
281 which the thickness increases by depth when a coarser mesh is required in the model (Figure 7). The whole model
282 consists of 1,200,000 elements including triangular elements and triangular prisms.

283 

284 3.1.2 Governing Equations

285 Heat transfer between the basements and the surrounding ground was captured by coupling and solving the
286 equations for heat transfer and fluid flow in a porous medium (ground). The governing equations, coupling
287 techniques and initial and boundary conditions used in this study were previously validated against experimental
288 data in a similar problem where heat transfer between the tunnel wall and the porous ground with groundwater
289 flow was investigated. Further details on validation of the coupling techniques and governing equations can be
290 found in Bidarmaghz (2014), Bidarmaghz and Narsilio (2018), Bidarmaghz et al. (2017), Makasis et al. (2018).

291 Heat conduction occurs in the ground and in the wall/floor of the basements. Unlike most of the literature
292 considering a higher ground thermal conductivity (effective thermal conductivity) representing the effects of
293 groundwater, the groundwater flow was numerically modelled in this study using Darcy's Law and heat
294 convection occurring in the ground due to the presence of groundwater and its flow is modelled in details. The
295 conductive-convective heat transfer equations can be expressed as follows (COMSOL, 2018a, Vahab et al., 2018):

$$(\rho C_p)_{eff} \frac{\partial T_m}{\partial t} + (\rho C_p \mathbf{v}_f) \nabla T_m + \nabla \cdot \mathbf{q} = 0 \quad 1$$

¹⁰ GeoInformation, (2017a). UK Buildings. Verisk Analytics.

$$q = \lambda_{eff} \nabla T_m \quad 2$$

$$(\rho C_p)_{eff} = (1 - n) \rho_m C_{p,m} + n \rho_f C_{p,f} \quad 3$$

$$\lambda_{eff} = (1 - n) \lambda_m + n \lambda_f \quad 4$$

296 where ρ_m represents the material density (i.e., ground, concrete, air), and $C_{p,m}$ and λ_m represent the specific heat
 297 capacity and thermal conductivity of the material respectively. Above, λ_f represents the thermal conductivity of
 298 the groundwater and λ_{eff} is the effective thermal conductivity of the porous ground. Note that other estimations
 299 may be used for λ_{eff} in Eq. 2; here we choose Eq. 4 for this. $C_{p,f}$ is the groundwater specific heat capacity, n is the
 300 porosity, and ρ_f is the groundwater density.

301 Single phase fluid flow in a porous medium (groundwater flow) is usually described by Darcy's law, which states
 302 that the Darcy velocity field, \mathbf{v}_f , is determined by the total head gradient, the fluid dynamic viscosity, μ_f , and the
 303 structure of the soil (Bear, 2012, COMSOL, 2018b, Todd, 1959):

$$\mathbf{v}_f = -\frac{K}{\mu_f} (\nabla p_f - \rho_f g \nabla Z) \quad \frac{K}{\mu_f} = \frac{k_h}{\rho_f g} \quad 5$$

304 where K is the isotropic permeability of the ground, p_f represents the pore pressure in the ground, ρ_f is the
 305 groundwater density, k_h is the hydraulic conductivity of the ground, \mathbf{g} is the gravitational acceleration vector, and
 306 μ_f is the groundwater dynamic viscosity.

307 Inserting Darcy's Law into the continuity equations produces the generalized governing equation:

$$\frac{\partial}{\partial t} (n\rho) + \nabla \cdot \rho \left[-\frac{K}{\mu_f} (\nabla p_f - \rho_f g \nabla Z) \right] = 0 \quad 6$$

308 Eqs. 5 and 6 are solved for \mathbf{v}_f and p_f in the ground and are coupled to Eq. 1 via \mathbf{v}_f .

309 3.1.3 Initial & Boundary Conditions

310 To solve the above system of equations, appropriate initial and boundary conditions are required as shown in
 311 Figure 7 and are summarized as follows:

- 312 • The groundwater velocity of 0.25m/day is assigned to the model by introducing a hydraulic head gradient
 313 to the ground farfield boundaries. This is taken from the available groundwater level contours reflecting
 314 the average hydraulic head difference in the southern part of the borough. A hydraulic head difference
 315 of about 10 m over 2 km of horizontal distance ($i_h=0.005$) is shown in RBKC's southern part (Figure 6).
 316 In the numerical models (with a horizontal distance of 1.5 km), the hydraulic head difference is adjusted
 317 to represent the same hydraulic gradient. To further study the effect of groundwater flow rate on heat
 318 transfer between the basements and the ground, flow rates of 0m/day (no flow), 0.5m/day and 1m/day
 319 are also considered¹¹ (Burke et al., 2014). The variations in groundwater flow rate is implemented by
 320 changing the hydraulic gradient in the models (from no flow to $i_h=0.01$ (0.5 m/day) and the extreme case
 321 of $i_h=0.02$ (1m/day).
- 322 • The basements' wall and floor are kept at the average indoor temperature in the UK (18°C) throughout
 323 the year¹².
- 324 • Thermal insulation is assigned to the building footprint on the surface to represent the thermally insulated
 325 building floor.

¹¹ Arup 2008. Royal Borough of Kensington and Chelsea Town Planning Policy on Subterranean Development: Phase1-Scoping Study. London, UK.

¹² How warm is your home, BBC Magazine, UK

- The undisturbed ground temperature is set at 12.5°C based on the temperature monitoring experiment in Earls’s Court, London (Price et al., 2018).
- The seasonal changes in ground temperature are modelled as a time and depth varying temperature. This temperature is applied as a depth varying initial temperature to the entire model including the farfield ground boundaries and as a time-varying temperature to the ground surface to account for surface temperature fluctuations (Baggs, 1983, Jensen-Page et al., 2018, Bidarmaghz et al., 2016):

$$T_{ground}(z, t) = T_{ground,mean} - 1.07 \cdot k_v \cdot A_s \cdot \exp(-0.00031552 \cdot z \cdot \alpha^{-0.5}) \cdot \cos\left(\left(\frac{2\pi}{365}\right) \cdot (t - t_0 + 0.018335 \cdot z \cdot \alpha^{-0.5})\right) \quad 7$$

where $T_{ground,mean}$ is the ground annual average temperature, (12.5°C). k_v is the vegetation coefficient set at 0.5 accounting for 50% vegetation cover for each area. A_s , 8.3°C, is the annual air swing temperature. t is the day of the year. z indicates the depth in the ground [m]. α is the ground diffusivity equal to an average value of $9.65 \times 10^{-7} \text{m}^2/\text{s}$, calculated based on physical and thermal properties of the soil presented in Table 2. t_0 is the coldest temperature day from January 1st (British Geological Survey, 2017, Price et al., 2018).

- The ground farfield boundary is set as thermal insulation instead of a time-depth varying temperature. In reality, the ground at farfield is also thermally disturbed when considering basements or other heat sources in adjacent areas. However, such thermal interference was not the focus of this proof-of-concept study.

A summary of the geological, physical and hydrothermal characteristics of the ground for the three areas modelled are presented in Table 2 (Busby et al., 2009, Price et al., 2018, British Geological Survey, 2017).

Table 2. Geological, physical and hydrothermal properties of the three areas shown in Figure 5.

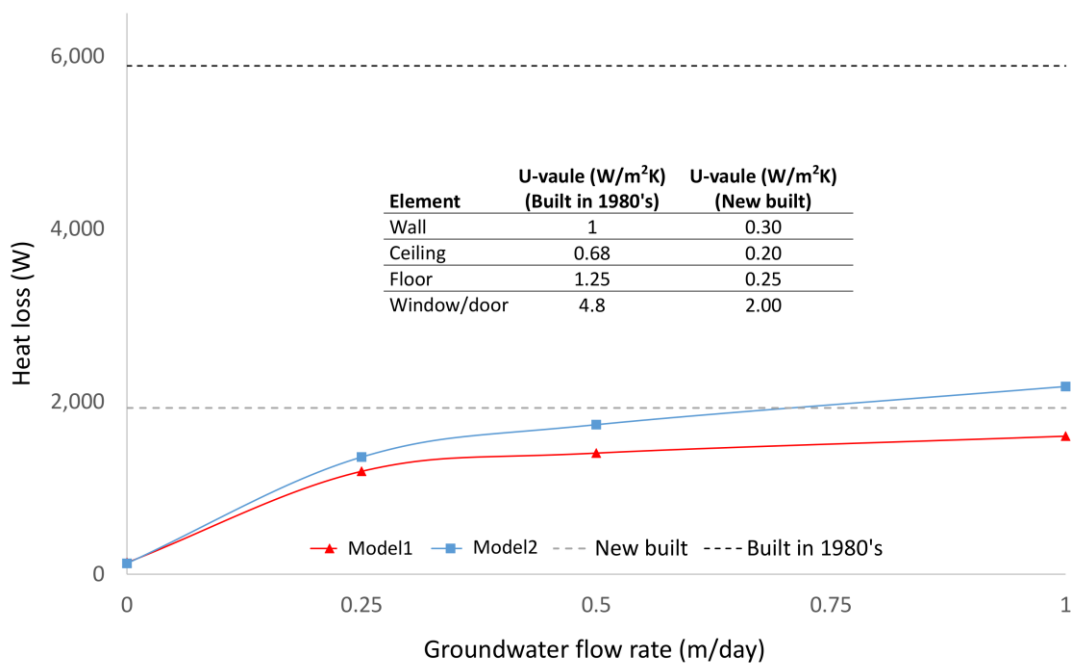
Model 1							
	<i>Geology</i>	λ [W/(mK)]	ρ [kg/m ³]	C_p [J/(kgK)]	<i>Porosity</i> [-]	k_h [m/s]	a [m ² /s]
0-2m	Kempton Park Gravel (unsaturated)	0.77	1,600	1,100	0.35	4.2×10^{-5}	4.5×10^{-7}
2-10m	Kempton Park Gravel (saturated)	2.5	1,900	1,440	0.35	5.6×10^{-4}	9.1×10^{-7}
10-90m	London Clay	1.7	2,000	870	0.5	1×10^{-9}	9.7×10^{-7}
Model 2							
	<i>Geology</i>	λ [W/(mK)]	ρ [kg/m ³]	C_p [J/(kgK)]	<i>Porosity</i>	k_h [m/s]	a [m ² /s]
0-2m	Kempton Park Gravel (unsaturated)	0.77	1,600	1,100	0.35	4.2×10^{-5}	4.5×10^{-7}
2-5m	Kempton Park Gravel (saturated)	2.5	1,900	1,440	0.35	5.6×10^{-4}	9.1×10^{-7}
5-90m	London Clay	1.7	2,000	870	0.5	1×10^{-9}	9.7×10^{-7}
Model 3							
	<i>Geology</i>	λ [W/(mK)]	ρ [kg/m ³]	C_p [J/(kgK)]	<i>Porosity</i>	k_h [m/s]	a [m ² /s]
0-90m	London Clay	1.7	2,000	870	0.5	1×10^{-9}	9.7×10^{-7}

346 **4. Results and Discussions**

347 Figure 8 shows the heat loss (W) from the wall and slab of one basement (10L×5W×3D) to the ground and its
 348 comparison to the heat loss from the above-ground structure of the buildings (house of 50m² floor area and 125m²
 349 of the exposed wall (from The Building Regulations, 2016). Depending on the thickness of the permeable layer
 350 and groundwater flow rate, the heat rejection rate from the basements to the ground may be significant and
 351 comparable to the amount of heat loss from the above-ground structure of a newly built building to the air. These
 352 results are within the range of heat fluxes reported in the work of Epting et al. (2013) and Menberg et al (2013),
 353 where basements are constructed in saturated ground (~10 W/m² on average) (Epting and Huggenberger, 2013,
 354 Menberg et al., 2013).

355 Groundwater flow rate has less influence on the amount of heat losses from the basements to the ground, when
 356 the ground mainly consists of permeable material (model 1). However, when the thickness of the permeable layer
 357 decreases (model 2), faster groundwater flow leads to larger heat loss from basements and can become a
 358 significant percentage of the total heat loss from a building.

359 Underground structures constructed in impermeable soil, for example, most of the London Tube line constructed
 360 within London Clay Formation, have a consistent heat rejection rate into the ground due to minimal to negligible
 361 groundwater flow. However, heat transfer between the underground structures and the ground becomes more
 362 complex when groundwater flow is present. Heat rejection from heated basements constructed in the shallow
 363 ground with groundwater flow (permeable sand and gravel) varies significantly based on the geological
 364 distribution, and thickness of the permeable layer as shown in Figure 8. Therefore, the thermal energy demand
 365 for basements also varies and it is necessary to gain a better understanding of the ground thermal status in order
 366 to develop an efficient energy system design for underground structures.

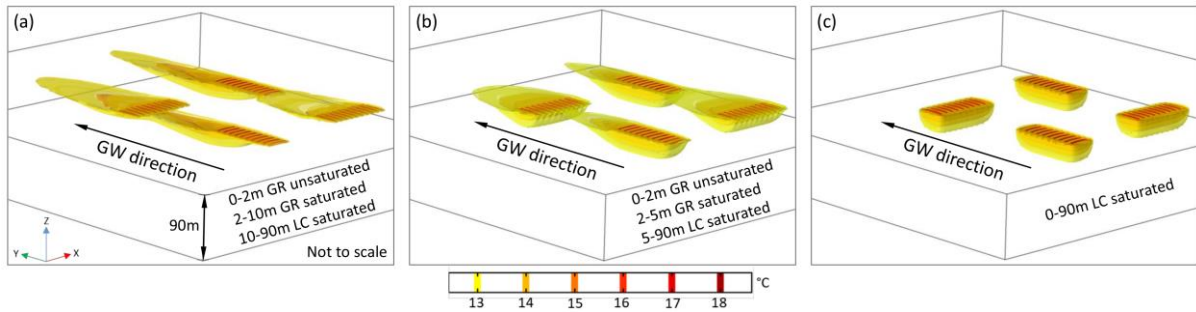


367
 368 Figure 8. Heat loss from basement wall and floor (one basement - 10L×5W×3D) for models 1 and 2 and for typical double
 369 storey building (50 m² of floor area and 125 m² of the exposed wall) based on recommended U-values in 1980's and 2016¹³.

370 Figure 9 shows the extent of the thermally affected ground with a temperature gradient of 1°C to 5.5°C with
 371 respect to the ground's annual average temperature (around 12.5°C) in vertical and horizontal directions in 25
 372 years. For example, in model 1, the deepest point in the ground with a temperature gradient (T>12.5°C) occurs

¹³ The Building Regulations 2016. Conservation of Fuel and Power in New Dwellings. England.

373 further away from the basement footprints in the direction of the groundwater flow and at the depth of 32m (Figure
 374 9-a). The high permeability of the ground in model 1 affects the concentration of the thermal disturbance around
 375 the basements and leads to a faster heat dissipation to the farfield. However, in model 2 and 3, the deepest point
 376 in the ground affected by the heated basements occurs at the depth of about 35m and 31m respectively (Figure
 377 9-b and c). The combination of permeable layer thickness and groundwater flow rate in model 1 results in a larger
 378 horizontal extent of the disturbed ground (~400m from edge of basements) in comparison to model 2 (~250m)
 379 and model 3 (~10m) over 25 years, due to its significantly low permeability, hence negligible groundwater
 380 movement. These results also show that the geothermal potential, its spatial concentration and extent also varies
 381 in the ground with different characteristics.



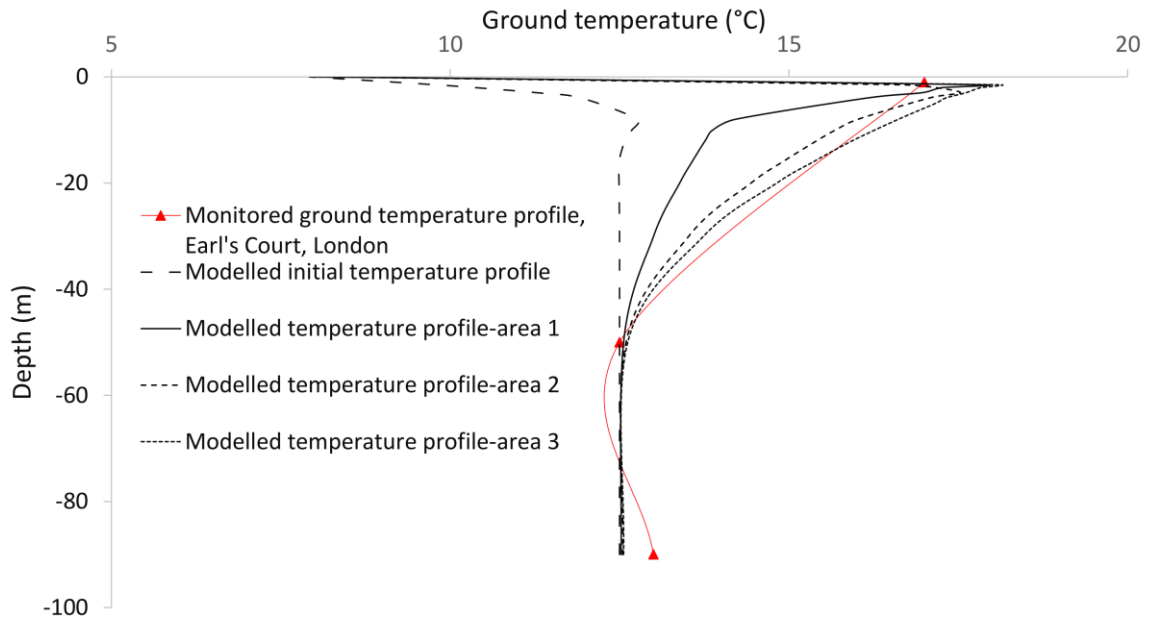
382

383

Figure 9. Thermally affected ground for 25 years with groundwater flow rate of 0.25m/day.

384 The modelled depth varying ground temperature profile - after 25 years of simulation - clearly shows the
 385 differences in ground temperature distributions for different models (see Figure 10). The variations in ground
 386 temperature gradient (thermal discharge rate) are related to the permeable layer thickness. The highest temperature
 387 gradient ($0.5^{\circ}\text{C}/\text{m}$) is observed for model 1 within the superficial deposit as shown in Figure 10. For model 2
 388 where the permeable layer thickness is smaller, the temperature gradient is about $0.3^{\circ}\text{C}/\text{m}$ for the first 5m
 389 (permeable layer). The temperature gradient is shown to be around 0.1°C for model 3, where the model consists
 390 of impermeable London Clay. It is also worth noting that depending on the thickness and thermal properties of
 391 the (superficial layer) permeable layer, the temperature gradient within the London Clay varies. This is due to the
 392 fact that the extent of thermal disturbance in the Clay is also dependent on the characteristics of the layer above.
 393 This is captured in the differences between temperature gradients in London Clay Formation for different models.

394 The limited available ground temperature measurements in Earl's Court, London is shown in Figure 10 (triangular
 395 marks (Price et al., 2018)). The Experimental ground temperature profile illustrates the general ground
 396 temperature trend by depth, which shows a relatively similar trend to the modelled temperature profile of models
 397 2 and 3. The geological variation of the field located in Earl's Court consists of about 4-5m of River Terrace
 398 Deposits underlain by London Clay. The exact location of the field is shown in Figure 5.



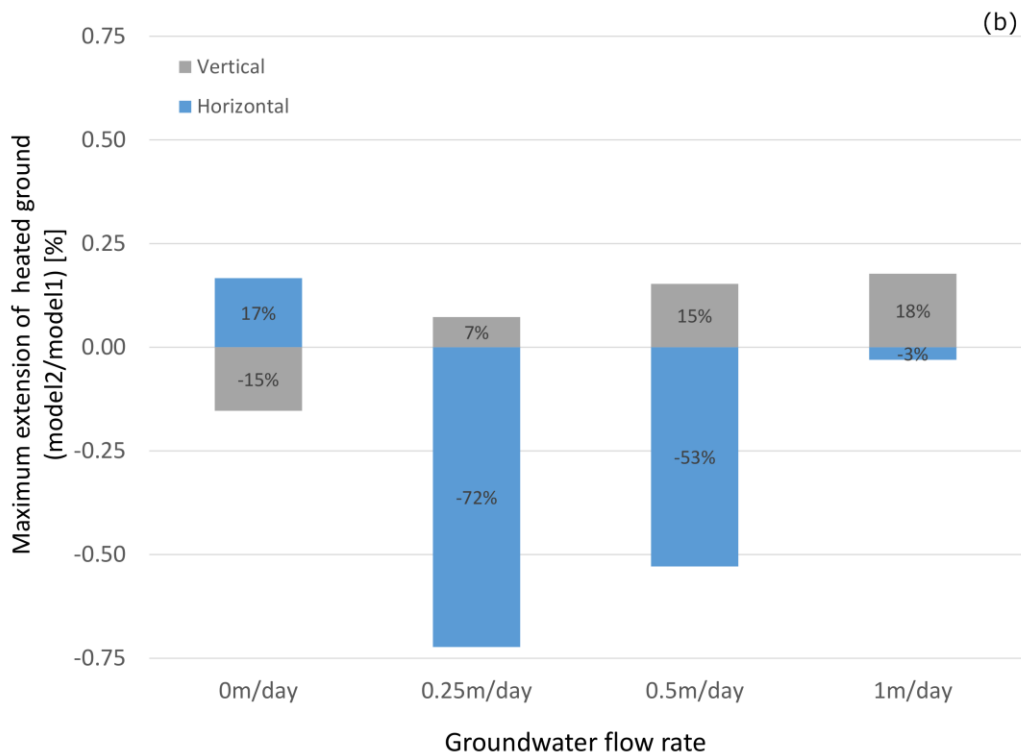
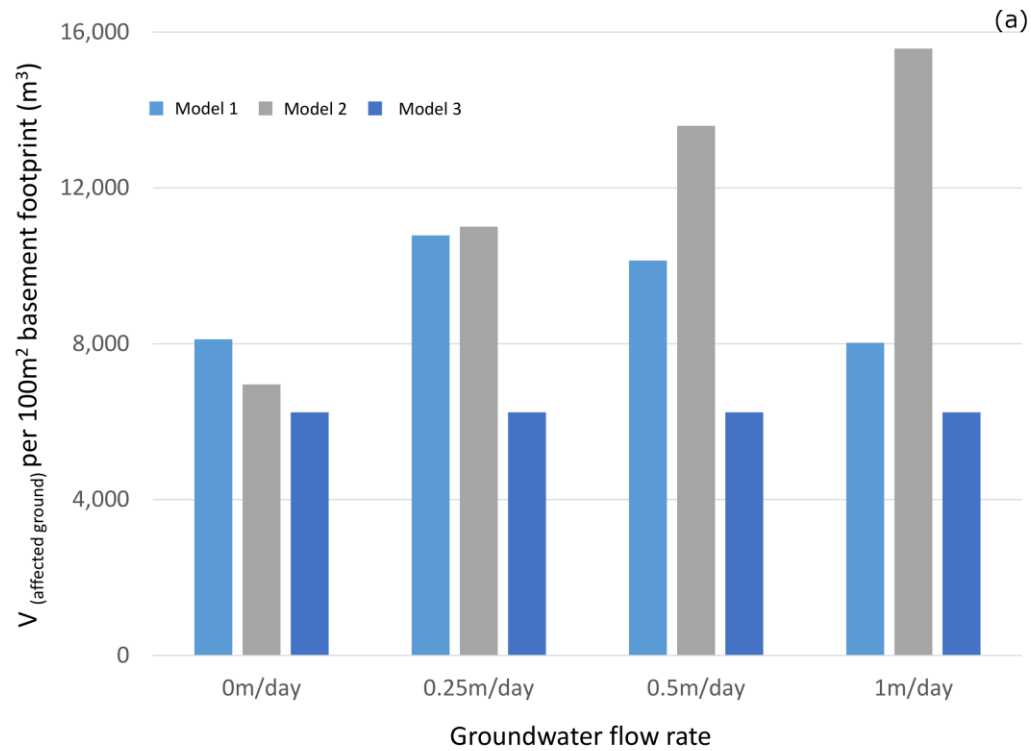
399
400

Figure 10. Measured and modelled temperature profiles.

401 Figure 11-a shows the volume of the ground with 1°C to 5.5°C temperature increase within 100m² of the basement
 402 footprint in 25 years. The volume of the thermally disturbed ground shows a non-consistent trend with an increase
 403 in groundwater flow rate. When the groundwater flow rate increases above 0.25m/day in model 1, the heat
 404 generated around the heated basements dissipates by the fast flow. In model 2, on the other hand, the volume of
 405 the disturbed ground consistently increases for faster flows as the ease of heat transport in the ground is affected
 406 by the smaller volume of granular material leading to the accumulation of heat in the ground surrounding the
 407 basements. As expected, the groundwater flow rate does not have a significant effect on model 3 due to the very
 408 low permeability of the clay material.

409 Figure 11-b shows the difference between model 2 and model 1 in terms of the maximum extent of the heated
 410 ground (with a temperature higher than the ground annual average temperature, 12.5°C) in the horizontal and
 411 vertical directions. In the horizontal direction, there is a significant difference with a relatively slow flow
 412 (0.25m/day) as model 1 extends 72% more in the horizontal direction than model 2. However, this difference
 413 decreases with an increase in groundwater flow rate, and at an extreme groundwater flow rate (1m/day) the
 414 difference is only about 3%. In ground with a large volume of permeable layer (e.g., model 1), any two points at
 415 certain horizontal distances from the basements show a smaller temperature gradient than in model 2 where the
 416 thickness of the granular layer decreases. This is because the heat rejected from the basements is carried further
 417 away from the basement structure, resulting in a maximum temperature gradient (18°C-12.5°C=5.5°C) occurring
 418 at a larger length of the ground at any depth. However, in the case of an extreme groundwater flow rate, this effect
 419 is minimised. Therefore, model 1 and 2 show a smaller difference in the horizontal extension of the thermally
 420 disturbed ground.

421 In the vertical direction, rejected heat from the basement is continuously dissipated in the direction of the
 422 groundwater flow in model 1 with largest volume of permeable material resulting in a shallower penetration depth
 423 of the heated area in the ground, which also decreases for faster groundwater flows (Figure 11-b).



424

425 Figure 11. The thermally affected volume of the ground per 100m² of basement footprint (a), The difference between the
 426 extension of the heated ground in horizontal and vertical directions between the model 1 and model 2 (b).

427 **5. Conclusions**

428 Reliable knowledge of ground thermal status in urban areas is crucial for 1) the sustainable development of
 429 underground structures, 2) the optimal utilization of geothermal sources and 3) efficient energy system design for

430 underground structures. To achieve such understanding, not only are the built environment and external
431 contributors (anthropogenic heat fluxes) to ground temperature rise important for consideration and study, but
432 also analysis that is based on a good understanding of the local geological and hydrogeological conditions is
433 required. The aim of this proof-of-concept study was to highlight the impact of geology and hydrogeology on heat
434 rejection rate from underground structures, and thus the extent of ground thermal disturbance. Numerical analysis
435 of a sample of selected areas shows that thermal losses from heated basements to the ground can constitute a
436 significant percentage of the total heat loss from a building, particularly in the presence of groundwater flow.
437 However, this is not a consistent trend. Results show that the influence of groundwater flow on thermal loss from
438 basements is less in ground with a large volume of permeable material. In addition, the extent of thermal
439 disturbance in the ground is also dependent on the combination of geological and hydrogeological characteristics.
440 In ground mainly consisting of permeable material, the volume of thermally affected ground shows an inverse
441 correlation with the groundwater flow rate. However, a direct correlation exists when the thickness of permeable
442 layer decreases. A larger horizontal to vertical ratio of ground thermal disturbance is observed when the thickness
443 of permeable layer increases.

444 The widely used assumption of constant annual average temperature for ground is demonstrated to be incorrect
445 by this study. This incorrect assumption of the ground temperature has a direct impact on the evaluation of the
446 energy requirements for basements. By using the ground as a source of geothermal energy, an accurate estimation
447 of the ground temperature facilitates and improves the sustainable utilization of geothermal energy sources.

448 The understanding of the evolution of ground temperature necessitates a large-scale study on the thermal
449 interaction between underground spaces and the surrounding ground. A city-scale model including different
450 underground sources of heat (basements, train tunnels, etc.) is therefore required and will be the focus of our
451 future work.

452 **6. Acknowledgement**

453 This work is funded under Global University Alliance (Cambridge Centre for Smart Infrastructure and
454 Construction, University of California, Berkeley, and National University of Singapore) and in collaboration with
455 British Geological Survey (BGS) (EPSRC reference: EP/N021614/1).

456 7. **References**

- 457 1. Un-Habitat 2012. *State of the World's Cities 2008/9: Harmonious Cities*, Routledge.
- 458 2. Price, S. J., Terrington, R. L., Busby, J., Bricker, S. & Berry, T. 2018. 3D ground-use optimisation for
459 sustainable urban development planning: A case-study from Earls Court, London, UK. *Tunnelling and*
460 *Underground Space Technology*, 81, 144-164.
- 461 3. Zhang, Y., Soga, K. & Choudhary, R. 2014. Shallow geothermal energy application with GSHPs at city
462 scale: study on the City of Westminster. *Géotechnique Letters*, 4, 125-131.
- 463 4. Arola, T. & Korkka-Niemi, K. 2014. The effect of urban heat islands on geothermal potential: examples
464 from Quaternary aquifers in Finland. *Hydrogeology Journal*, 22, 1953-1967.
- 465 5. Zhu, K., Blum, P., Ferguson, G., Balke, K.-D. & Bayer, P. 2010. The geothermal potential of urban heat
466 islands. *Environmental Research Letters*, 5, 044002.
- 467 6. Benz, S. A., Bayer, P., Goettsche, F. M., Olesen, F. S. & Blum, P. 2015a. Linking surface urban heat
468 islands with groundwater temperatures. *Environmental science & technology*, 50, 70-78.
- 469 7. Menberg, K., Blum, P., Schaffitel, A. & Bayer, P. 2013. Long-term evolution of anthropogenic heat fluxes
470 into a subsurface urban heat island. *Environmental science & technology*, 47, 9747-9755.
- 471 8. Herbert, A., Arthur, S. & Chillingworth, G. 2013. Thermal modelling of large scale exploitation of ground
472 source energy in urban aquifers as a resource management tool. *Applied energy*, 109, 94-103.
- 473 9. Barla, M., Donna, A. D. & Baralis, M. J. E. G. 2018. City-scale analysis of subsoil thermal conditions due
474 to geothermal exploitation. 1-11.
- 475 10. Attard, G., Winiarski, T., Rossier, Y. & Eisenlohr, L. 2016a. Impact of underground structures on the flow
476 of urban groundwater. *Hydrogeology journal*, 24, 5-19.
- 477 11. Epting, J. & Huggenberger, P. 2013. Unraveling the heat island effect observed in urban groundwater
478 bodies—Definition of a potential natural state. *Journal of hydrology*, 501, 193-204.
- 479 12. Benz, S. A., Bayer, P., Menberg, K., Jung, S. & Blum, P. 2015b. Spatial resolution of anthropogenic heat
480 fluxes into urban aquifers. *Science of The Total Environment*, 524, 427-439.
- 481 13. Attard, G., Rossier, Y., Winiarski, T. & Eisenlohr, L. 2016b. Deterministic modeling of the impact of
482 underground structures on urban groundwater temperature. *Science of The Total Environment*, 572, 986-
483 994.
- 484 14. Taniguchi, M., Shimada, J., Fukuda, Y., Yamano, M., Onodera, S.-i., Kaneko, S. & Yoshikoshi, A. 2009.
485 Anthropogenic effects on the subsurface thermal and groundwater environments in Osaka, Japan and
486 Bangkok, Thailand. *Science of the total environment*, 407, 3153-3164.
- 487 15. Ferguson, G. & Woodbury, A. D. 2007. Urban heat island in the subsurface. *Geophysical research letters*,
488 34.
- 489 16. Ferguson, G. & Woodbury, A. D. 2004. Subsurface heat flow in an urban environment. *Journal of*
490 *Geophysical Research: Solid Earth*, 109.
- 491 17. Epting, J., García-Gil, A., Huggenberger, P., Vázquez-Suñe, E. & Mueller, M. H. 2017. Development of
492 concepts for the management of thermal resources in urban areas—Assessment of transferability from the
493 Basel (Switzerland) and Zaragoza (Spain) case studies. *Journal of hydrology*, 548, 697-715.
- 494 18. Epting, J., Händel, F., Huggenberger, P. J. H. & sciences, e. s. 2013. Thermal management of an
495 unconsolidated shallow urban groundwater body. 17, 1851-1869.
- 496 19. Mueller, M. H., Huggenberger, P. & Epting, J. 2018. Combining monitoring and modelling tools as a basis
497 for city-scale concepts for a sustainable thermal management of urban groundwater resources. *Science of*
498 *The Total Environment*, 627, 1121-1136.
- 499 20. Rivera, J., Blum, P. & Bayer, P. 2017. Increased ground temperatures in urban areas: Estimation of the
500 technical geothermal potential. *Renewable Energy*, 103, 388-400.
- 501 21. Vázquez Suñe, E., Marazuela Calvo, M. Á., Velasco Mansilla, D. V., Diviu, M., Perez Estaun, A. &
502 Álvarez Marrón, J. J. S. E. 2016. A geological model for the management of subsurface data in the urban
503 environment of Barcelona and surrounding area. 7, 1317-1329.

- 504 22. Furfano, D., Liebson, R. & Brown, R. 2018. Now subway platform temperature feels like hell, too. *New York Post*.
505
- 506 23. Ampofo, F., Maidment, G. & Missenden, J. 2004. Underground railway environment in the UK Part 2: Investigation of heat load. *Applied Thermal Engineering*, 24, 633-645.
507
- 508 24. Cockram, L. J. & Birnie, G. R. the ventilation of London underground railways. 2nd International Symposium on the Aerodynamics and Ventilation of Vehicle Tunnels, 1976 Cambridge, England.
509
- 510 25. Barla, M., Di Donna, A. & Perino, A. J. G. 2016. Application of energy tunnels to an urban environment. 61, 104-113.
511
- 512 26. Baldwin, S., Holyord, E. & Burrows, R. 2018. Mapping the Subterranean Geographies of Plutocratic London: Luxified Troglodytism?
513
- 514 27. Angelotti, A., Alberti, L., La Licata, I. & Antelmi, M. Borehole Heat Exchangers: heat transfer simulation in the presence of a groundwater flow. *Journal of Physics: Conference Series*, 2014. IOP Publishing, 012033.
515
516
- 517 28. Hecht-Méndez, J., De Paly, M., Beck, M., Bayer, P. J. E. c. & management 2013. Optimization of energy extraction for vertical closed-loop geothermal systems considering groundwater flow. 66, 1-10.
518
- 519 29. British Geological Survey. 2017. *RE: Ground Thermal and Hydraulic Property Data*.
- 520 30. Burke, H., Mathers, S., Williamson, J., Thorpe, S., Ford, J. & Terrington, R. 2014. The London Basin superficial and bedrock LithoFrame 50 Model.
521
- 522 31. Mathers, S., Burke, H., Terrington, R., Thorpe, S., Dearden, R., Williamson, J. & Ford, J. 2014. A geological model of London and the Thames Valley, southeast England. *Proceedings of the Geologists' Association*, 125, 373-382.
523
524
- 525 32. Kessler, H., Mathers, S. & Sobisch, H.-G. 2009. The capture and dissemination of integrated 3D geospatial knowledge at the British Geological Survey using GSI3D software and methodology. *Computers & geosciences*, 35, 1311-1321.
526
527
- 528 33. Jones, L. & Hulbert, A. 2017. User Guide for the Shrink-Swell 3D (GeoSure Extra) dataset V1.0. *In*: LEE, K. (ed.). Keyworth, Nottingham, UK: British Geological Survey.
529
- 530 34. McKenzie, A. 2015. User guide for the British Geological Survey National Depth to Groundwater Dataset.
- 531 35. Busby, J., Lewis, M., Reeves, H. & Lawley, R. 2009. Initial Geological Considerations Before Installing Ground Source Heat Pump Systems. *Quarterly Journal of Engineering Geology and Hydrogeology*, 42, 295-306.
532
533
- 534 36. Bidarmaghz, A. 2014. *3D numerical modelling of vertical ground heat exchangers*. PhD Thesis, The University of Melbourne.
535
- 536 37. Bidarmaghz, A. & Narsilio, G. 2018. Heat exchange mechanisms in energy tunnel systems. *Geomechanics for Energy and the Environment*.
537
- 538 38. Bidarmaghz, A., Narsilio, G. A., Buhmann, P., Moormann, C. & Westrich, B. 2017. Thermal Interaction Between Tunnel Ground Heat Exchangers and Borehole Heat Exchangers. *Geomechanics for Energy and the Environment*, 10, 29-41.
539
540
- 541 39. Makasis, N., Narsilio, G. A., Bidarmaghz, A. & Johnston, I. W. 2018. Ground-source heat pump systems: the effect of variable pipe separation in ground heat exchangers. *Computers and Geotechnics*, 100, 97-109.
542
- 543 40. COMSOL. 2018a. *Heat Transfer Module User's Guide* [Online].
- 544 41. Vahab, M., Akhondzadeh, S., Khoei, A. & Khalili, N. 2018. An X-FEM investigation of hydro-fracture evolution in naturally-layered domains. *Engineering Fracture Mechanics*, 191, 187-204.
545
- 546 42. Bear, J. 2012. *Hydraulics of groundwater*, Courier Corporation.
- 547 43. COMSOL. 2018b. *Subsurface Flow Module User's Guide* [Online].
- 548 44. Todd, D. K. 1959. *Ground water hydrology*, John Wiley and Sons, Inc, New York.
- 549 45. Baggs, S. A. 1983. Remote prediction of ground temperature in Australian soils and mapping its distribution. *Solar Energy*, 30, 351-366.
550

- 551 46. Jensen-Page, L., Narsilio, G. A., Bidarmaghz, A. & Johnston, I. W. J. R. e. 2018. Investigation of the effect
552 of seasonal variation in ground temperature on thermal response tests. 125, 609-619.
- 553 47. Bidarmaghz, A., Narsilio, G., Johnston, I. & Colls, S. 2016. The importance of surface air temperature
554 fluctuations on long-term performance of vertical ground heat exchangers. *Geomechanics for Energy and*
555 *the Environment*, 6, 35-44.
- 556
- 557